Supplementary Information

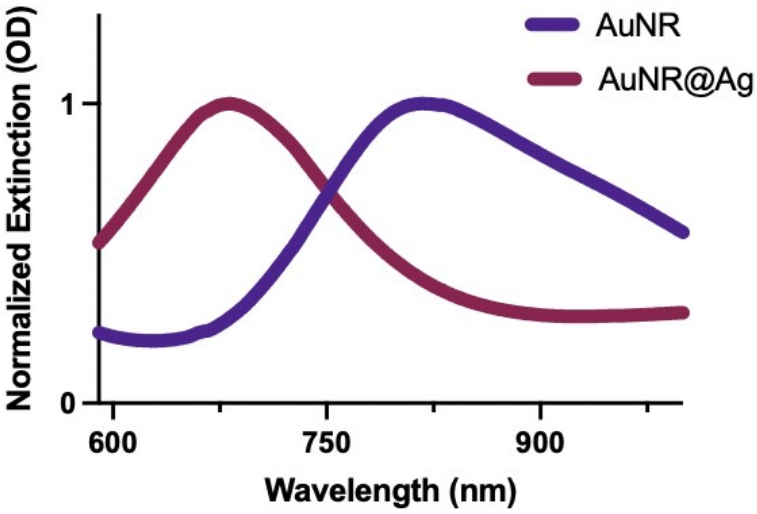

Figure S1. Absorbance spectra of the silver coating of the AuNR demonstrating a shift from 820 nm to 687 nm after synthesis

Table 1. Tabulated Nanorod Dimensions

Particle	Feret	Feret Δ	MinFeret	MinFeret Δ	Aspect Ratio
AuNR@Ag	30.36063	6.05123	13.05917	4.95795165	2.324851

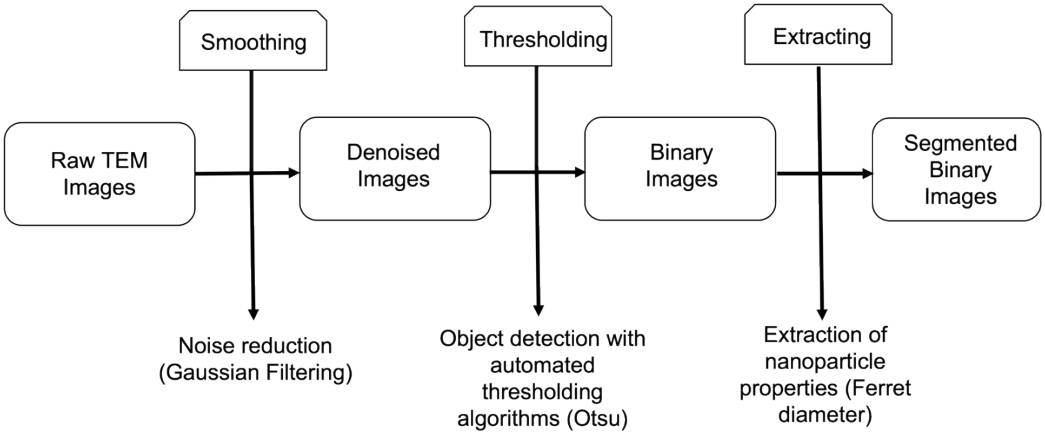

Figure S2: Data flow pipeline for automated thresholding and segmenting of nanorods.

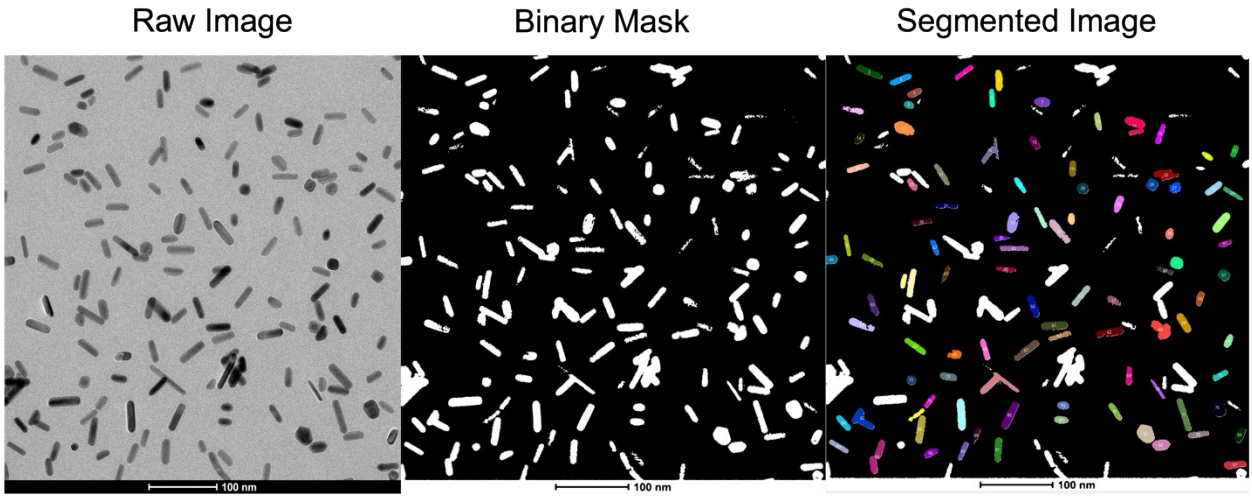

Figure S3. TEM image transformed to a binary mask and subsequently segmented for nanorods filtered by area size.

Table 2. Plasmonic properties comparing gold nanoparticles and silver coated nanoparticles at the 505 cm^{-1} peak.

Sample	**Absorption (nm)**	**SERS Enhancement (counts)**
AuNR	820 nm	5301.5
AuNR@Ag	687 nm	655.7

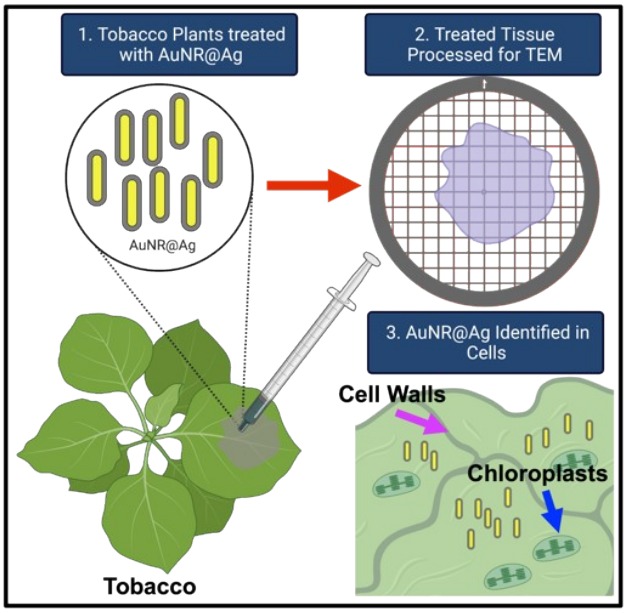

Supplementary Schematic 1. Illustration depicting TEM experimental workflow for localizing AuNR@Ag inside of tobacco plants. The purple arrows indicate cell walls, and the blue arrows show the chloroplasts inside of a cell.

Figure S4. Transmission electron microscopy micrograph of a tobacco leaf section treated with AuNR@Ag. Red boxes indicate the areas that were imaged at higher magnifications in Figure 2.

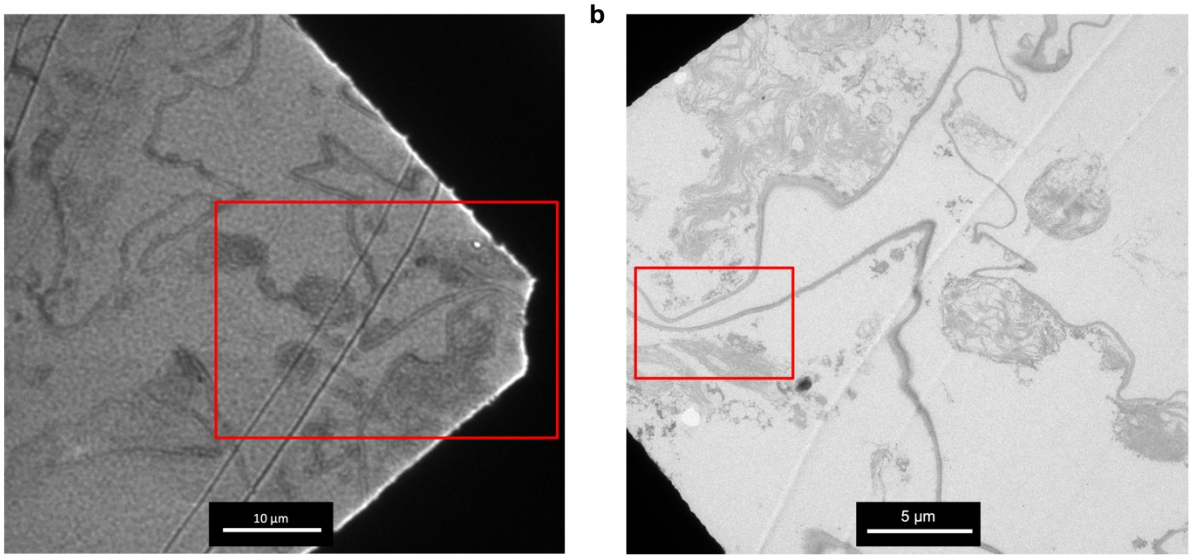

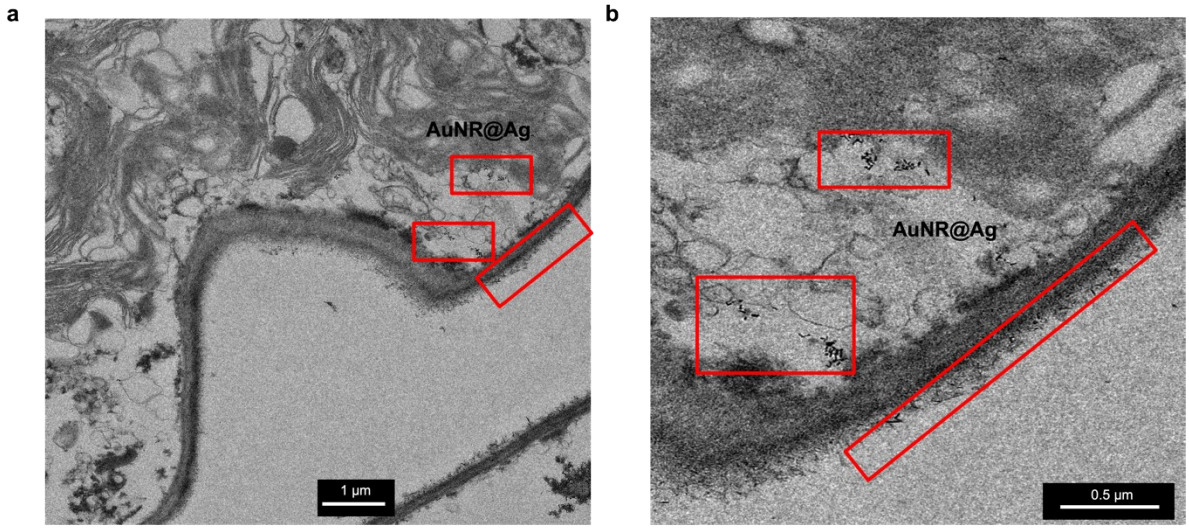

Figure S5. Transmission electron microscopy micrograph of a tobacco leaf section treated with AuNR@Ag. Red boxes indicate the areas where the AuNR@Ag are present. (B) Higher magnification section of (A).

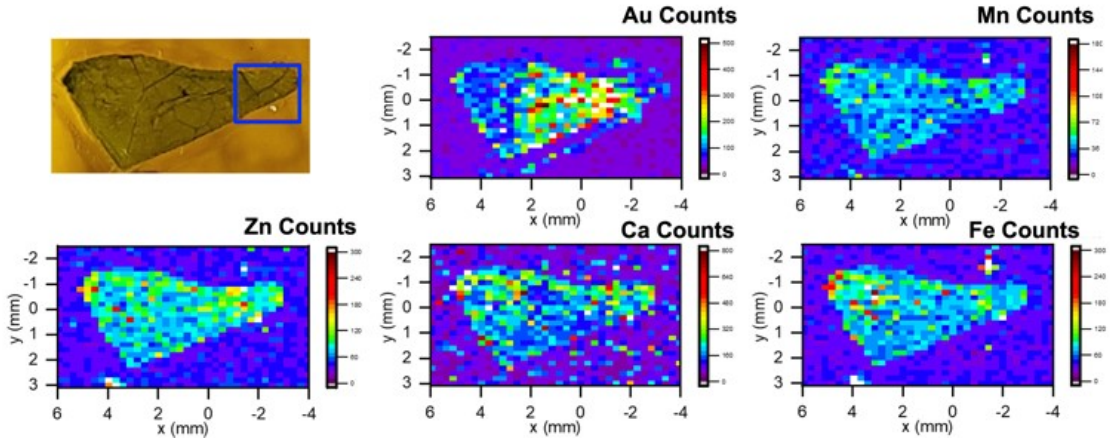

Figure S6. XRF maps demonstrating the distribution of different elements in the leaf, including gold from the AuNR@Ag infiltrated into the leaf.

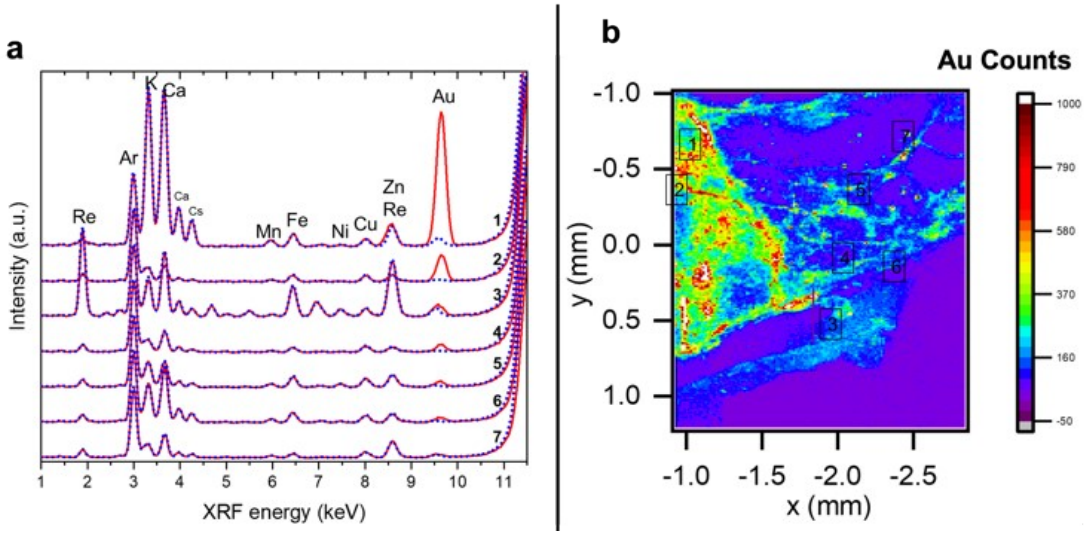

Figures S7. (a) XRF spectra from the numbered locations on the Au map of the leaf in the right (b) panel. Red line is with a probe energy above the Au LIII edge (at 12,000eV), blue dotted line is below the Au edge (at 11,900 eV). The top-right corner of the box around each number in the map points to the pixel at which the corresponding MCA scan was taken.

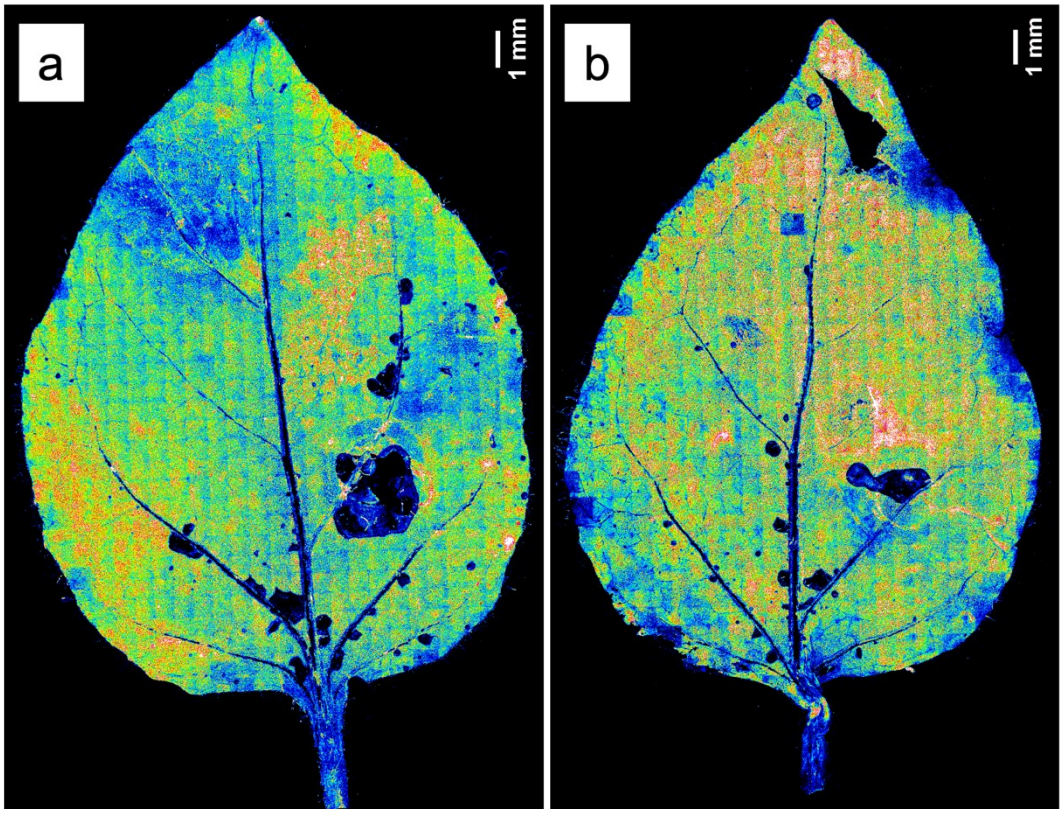

Figure S8. Two photon luminescence images of two whole leaf samples treated with AuNR@Ag (A), (B) with 800nm excitation and detection in the 400-500 nm range. Leaves were scanned in x, y and z using 25x objective. The maximum projection of the z-stack is displayed.

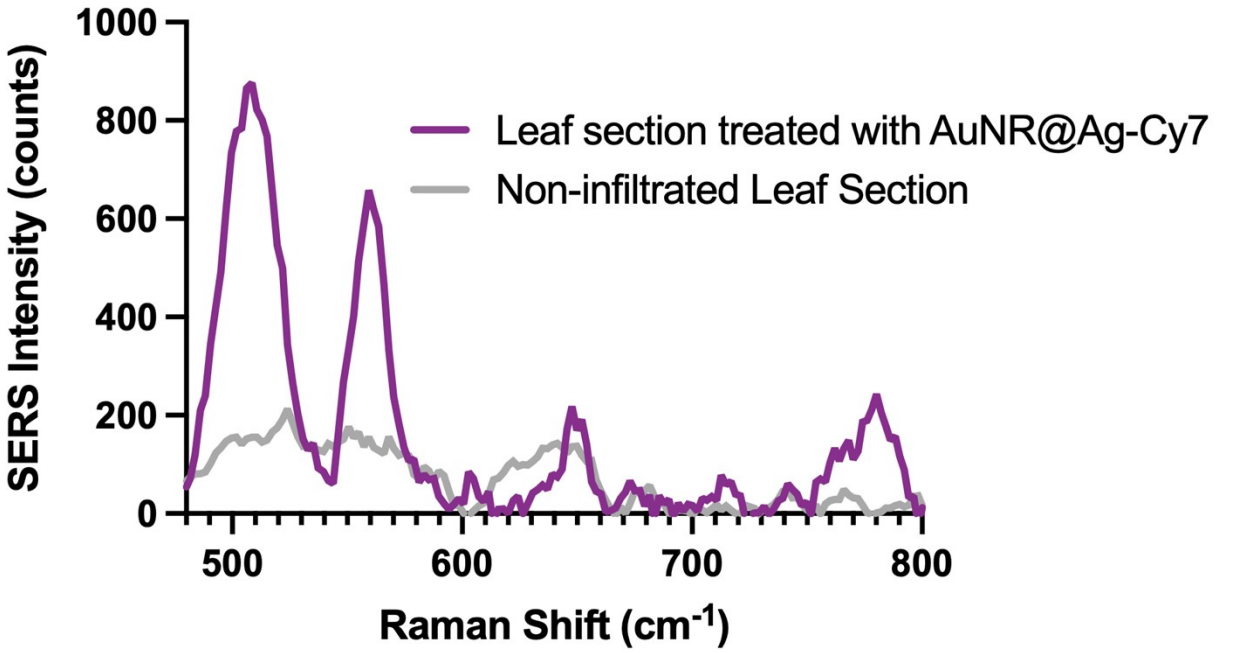

Figure S9. Raman spectra showing the difference between leaf tissue infiltrated with AuNR@Ag-Cy7 and tissue not treated with particles. The characteristic peaks at 505 & 558 cm^{-1} are only evident in the tissue treated with AuNR@Ag-Cy7.

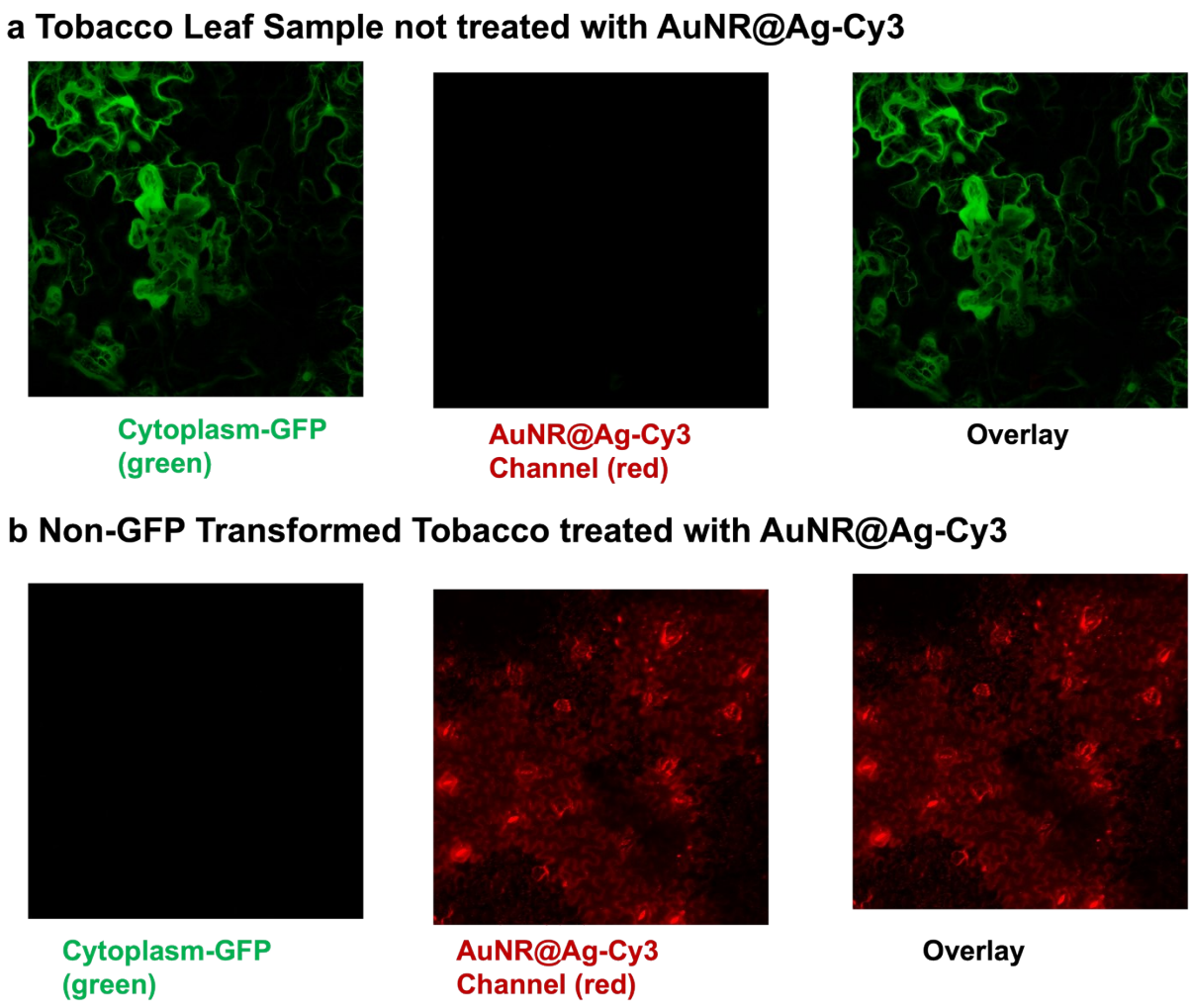

Figure S10. GFP expressing tobacco leaf not treated with nanoparticles (B) Tobacco leaf not transformed to express GFP infiltrated with AuNR@Ag-Cy3.

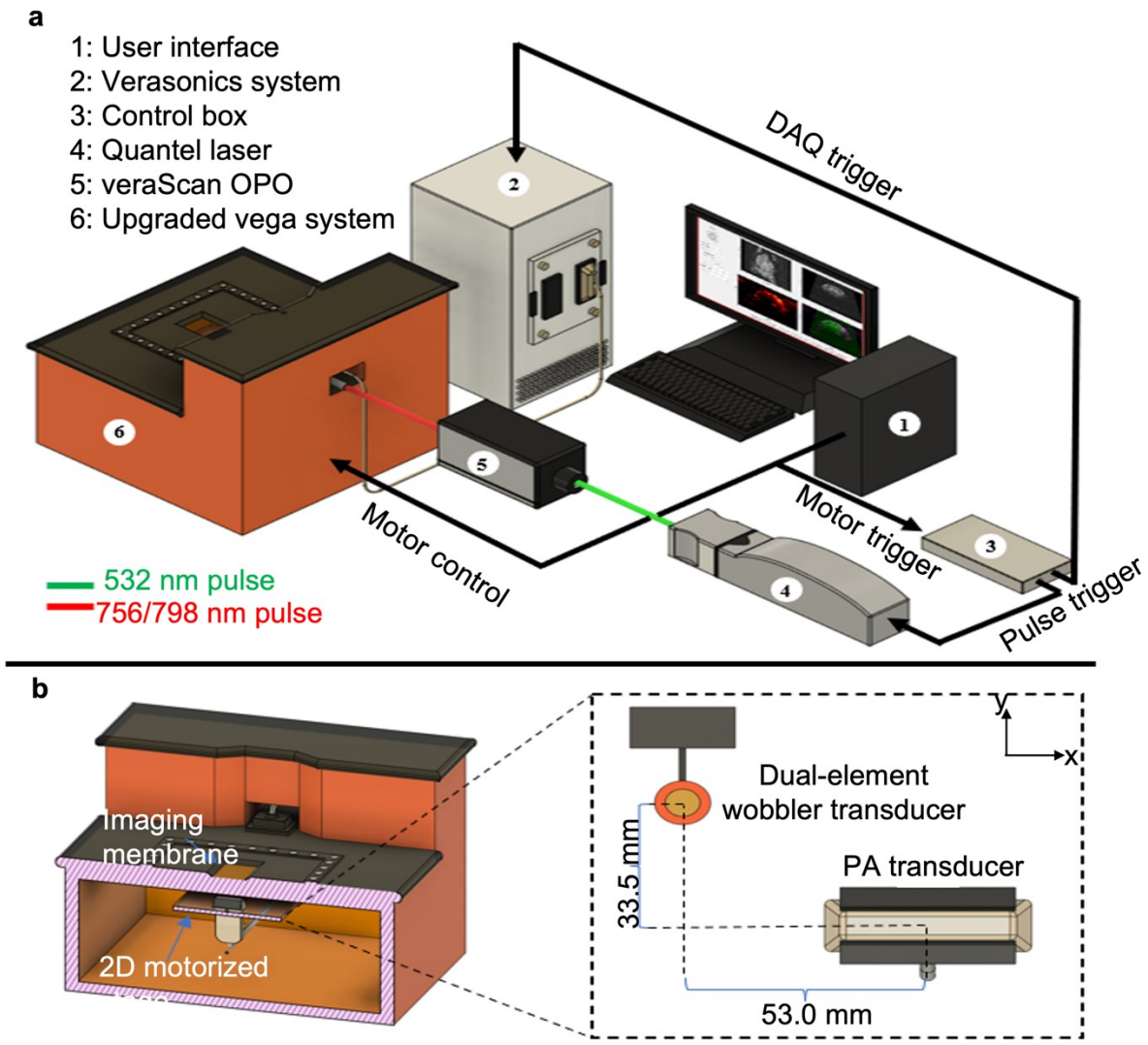

Figure S11. PA and US imaging system design. (a) Arrangement of PA imaging components. (b) The inside view of the PA and US imaging system, including a dual-element wobbler transducer for B-mode ultrasound (US) and a linear-array transducer with bilateral laser excitation for photoacoustic computed tomography (PACT). Both transducers are mounted on the same motorized stage with a fixed distance, allowing for automatic co-registration of images.

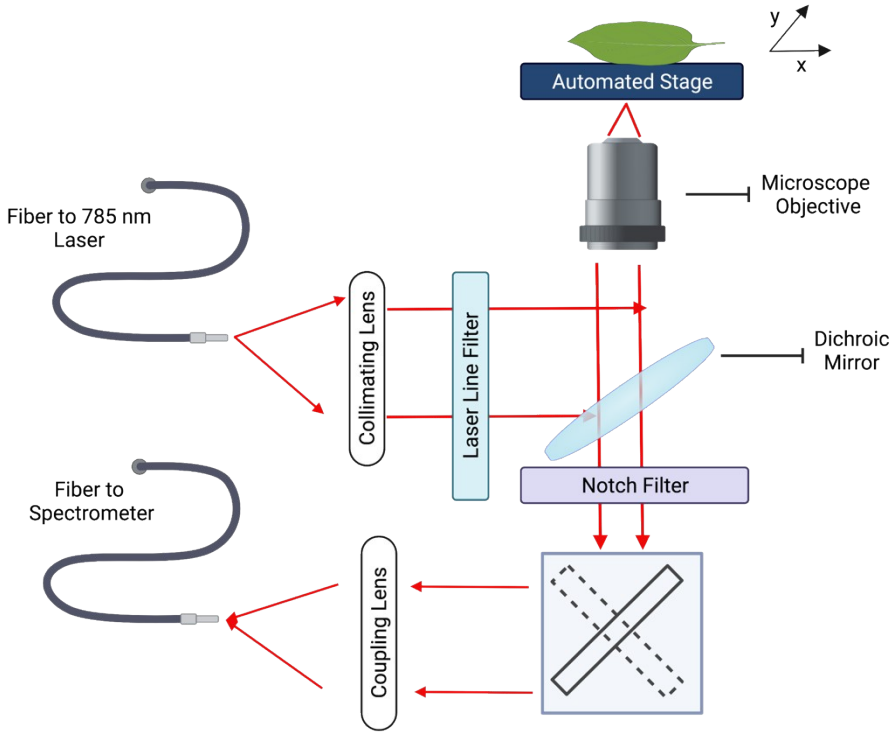

Figure S12. Point Scan and SERS setup schematic used to acquire SERS spectra and maps of the leaves treated with AuNR@Ag.

Supplementary Note 1

The 3D spatial resolution for the confocal XRF images shown in Figure 5 is 2x2x2 microns^3 and is described in Experimental Section 4. 2x2x2 micron^3 voxel resolution is capable of delineating individual cells that are ~100-microns in size. There was not temporal component for the XRF-based measurements as the sample was freeze-dried into a static state.

The spatial resolution of the photoacoustic system is approximately 0.45 mm along the lateral axis, 0.35 mm along the axial axis, and 1.7 mm along the elevational axis. At a single cross-sectional 2D imaging slice, the temporal resolution of photoacoustic imaging is generally limited by the laser repetition rate (in our case, 10 Hz). The spatial resolution of the B-mode ultrasound imaging is approximately 0.35 mm along the lateral axis, 0.15 mm along the axial axis, and 0.38 mm along the elevational axis. A complete 3D B-mode ultrasound scan of the leaf takes approximately 1 minute.

The best spatial resolution of the TPL system using a 25x objective is sub-micron in plane and ~1.1um (FWHM) out of plane or in the z-direction.[1] Thus, this system can resolve single cells as well as large cellular structures such as nuclei and vacuoles. The temporal resolution can be as fast as ~30 frames per second (512x512 images). This is enough for more precise temporal examination of biochemical pathways, which has previously been studied on the timescale of hours to days.[2, 3]

TPL could be combined with Raman confocal microscopy to simultaneously track nanoprobe location and SERS signal to investigate intracellular biochemical pathways in real-time. Raman mapping in this work has a spatial resolution that corresponds 600 µm with a field of view of 6 mm, although higher resolutions have been achieved previously by our group 200 µm.[4] The temporal resolution of the technique depends on the rate of the acquisition of the SERS measurement which averages 5 minutes.

Supplementary Note 2

Raman mapping of the SERS nanoprobes is designed to provide specific spectral information from dyes and biomolecules coated on the AuNR@Ag, but are not used to detect intracellular distribution of nanorods within the leaf; this information is provided by XRF and TPL which have been used for normalization. Comparatively, TPL has the best z-axis resolution and excellent x-y resolution, and would thus be able to more precisely determine intracellular nanoprobe location, as well as distinguishing nanoprobes in different layers of plant cells.

Photoacoustic imaging, on the other hand, can provide 3D information of the optical absorption of molecules with spatial resolution and penetration depth comparable to that of ultrasound imaging. Furthermore, photoacoustic imaging can achieve penetration depths on the order of 1 cm, which is advantageous for imaging thicker parts of the plant such as stems or roots. This allows for the study of the biodistribution of both endogenous and exogenous molecules in-vivo and at many excitation wavelengths. Advantages of Raman mapping include the unique spectral fingerprint that is collected allowing for the distinguishing of biomolecules or dyes coated on a metallic biosensor. The SERS effect can increase Raman signals by many orders of magnitude and the production of sharp Raman peaks from molecules facilitate its use for multiplex biochemical analyses in a wide variety of biochemical applications. X-ray fluorescence imaging can achieve cellular resolution imaging and is the only technique that can provide an elemental analysis of the sample and AuNR@Ag.

References

1. P. Vesely, *Scanning*, 2007, **29**, 91-91.
2. A. Raza Naqvi, S. Haseeb Khan, D. Mittal, H. Alshaya, M. Kazi and M. Sarwat, *Saudi Journal of Biological Sciences*, 2022, DOI: https://doi.org/10.1016/j.sjbs.2022.01.029, 103157.
3. F. Betti, M. J. Ladera-Carmona, D. A. Weits, G. Ferri, S. Iacopino, G. Novi, B. Svezia, A. B. Kunkowska, A. Santaniello, A. Piaggesi, E. Loreti and P. Perata, *Nature Plants*, 2021, **7**, 1379-1388.
4. B. M. Crawford, P. Strobbia, H. N. Wang, R. Zentella, M. I. Boyanov, Z. M. Pei, T. P. Sun, K. M. Kemner and T. Vo-Dinh, *ACS Appl. Mater. Interfaces*, 2019, **11**, 7743-7754.